

Supplementary Material

Contents

- 1. Alternative designations, celestial coordinates and apparent magnitudes**
- 2. Stellar properties**
- 3. Data preparation and transit modeling**
- 4. Kepler data validation**
- 5. Follow-up observations**
- 6. False positive analysis**
- 7. Coplanarity**
- 8. Orbital stability**
- 9. Formation**

1. Alternative designations, celestial coordinates and apparent magnitudes

Kepler-186 has the Kepler Input Catalog (KIC) designation 8120608 and coordinates RA=19:54:36.65 and Dec.=45:57:18.1 (J2000). The Kepler project has designated this star Kepler Object of Interest (KOI) 571. Planets b-f have KOI numbers KOI 571.03, .01, .02, .04 and .05. KOI numbers are assigned chronologically with discovery date, hence the inner planet (Kepler-186b) was discovered after planets c and d. The star has a brightness in the Kepler bandpass of $Kp=14.625$, Sloan magnitudes of $g=16.049$, $r=14.679$ and $i=14.015$ and infrared magnitudes of $J=12.473$, $H=11.823$ and $K=11.605$.

2. Stellar properties

Kepler-186 was observed as part of a spectroscopic campaign to characterize the cool KOIs (8) using the TripleSpec Spectrograph on the 200-inch Hale Telescope at Palomar Observatory. Effective temperature and metallicity were measured using the equivalent widths of the Na I and Ca I lines, as well as by measuring the H20-K2 index (38). For Kepler-186 the analysis yielded $T_{\text{eff}} = 3761 \pm 77$ K and $[Me/H] = -0.21 \pm 0.11$ dex, which we adopted to begin our analysis. From our transit modeling effort described in Section 3, we determine a mean stellar density of 4.9 ± 1.1 g cm^{-3} . To derive interior properties (such as radius, mass and luminosity) of the host star we used a grid of Dartmouth stellar isochrones (39) interpolated to a step size of 0.02 dex in metallicity. The observational constraints on the temperature, metallicity, and mean stellar density were fitted to the isochrones to derive the best-fitting model and $1-\sigma$ uncertainties (Table S1).

Interior models of cool main-sequence stars such as Kepler-186 are well known to show systematic differences to empirically measured stellar properties, with models between $0.3-0.8 M_{\odot}$ underestimating radii by up to 10-20% (14-16). It has been suspected that these differences are due

to enhanced magnetic activity in close binary systems, which can inhibit the efficiency of surface convection (40) or cause biases in modeling light curves of heavily spotted stars (41). While recent observations have indeed revealed evidence for better agreement in long-period, detached eclipsing binary systems (42, 43), angular diameter measurements of single M-dwarfs from optical long-baseline interferometry still show significant discrepancies (44). It is therefore unclear whether evolutionary models are adequate to derive accurate radii of M-dwarfs, and it is important to account for these discrepancies for the derived properties of detected planets (45).

Figure S1 shows Dartmouth models in a radius versus effective temperature diagram together with the observational $1-\sigma$ constraints from the mean stellar density and metallicity. The best-fitting model for Kepler-186 is shown in black, and a sample of stars with interferometric temperatures and radii is shown in red. As expected, empirically measured radii at the measured temperature for Kepler-186 are typically higher than the result derived from model isochrones. To take into account these discrepancies, we have added a 10% uncertainty in quadrature to our stellar radius and mass estimate for Kepler-186, yielding our final estimates of $M_{\star} = 0.48 \pm 0.05 M_{\odot}$ and $R_{\star} = 0.47 \pm 0.05 R_{\odot}$. Using the empirical $R-T_{\text{eff}}$ relation (46) would result in a radius of $0.51 R_{\odot}$ for Kepler-186, which would translate into a radius of $1.19 R_{\oplus}$ for Kepler-186f. Despite being slightly larger, such a radius would still place Kepler-186f well within the regime of plausibly rocky planets (23). We hence conclude that systematic differences between models and empirical observations for cool stars do not have a significant influence on the main conclusions of the paper.

Table S1. Stellar Characteristics

Parameter	Median	$\pm 1-\sigma$
$M_{\star} (M_{\odot})$	0.478	0.055
$R_{\star} (R_{\odot})$	0.472	0.052
Me/H (dex)	-0.28	0.10
$T_{\text{eff}} (\text{K})$	3788	54
L_{\star}/L_{\odot}	0.0412	0.0090
$\log g (\text{cm}^2 \text{s}^{-1})$	4.770	0.069
Distance (pc)	151	18

Note: The temperature and metallicity were initially derived from K-band spectroscopy and combined with the mean stellar density that we measured from the transit model to derive the interior properties of the star using a Monte Carlo simulation that utilized Dartmouth stellar isochrones. The distance was calculated assuming a line-of-sight extinction of 0.04 magnitudes in the J-band.

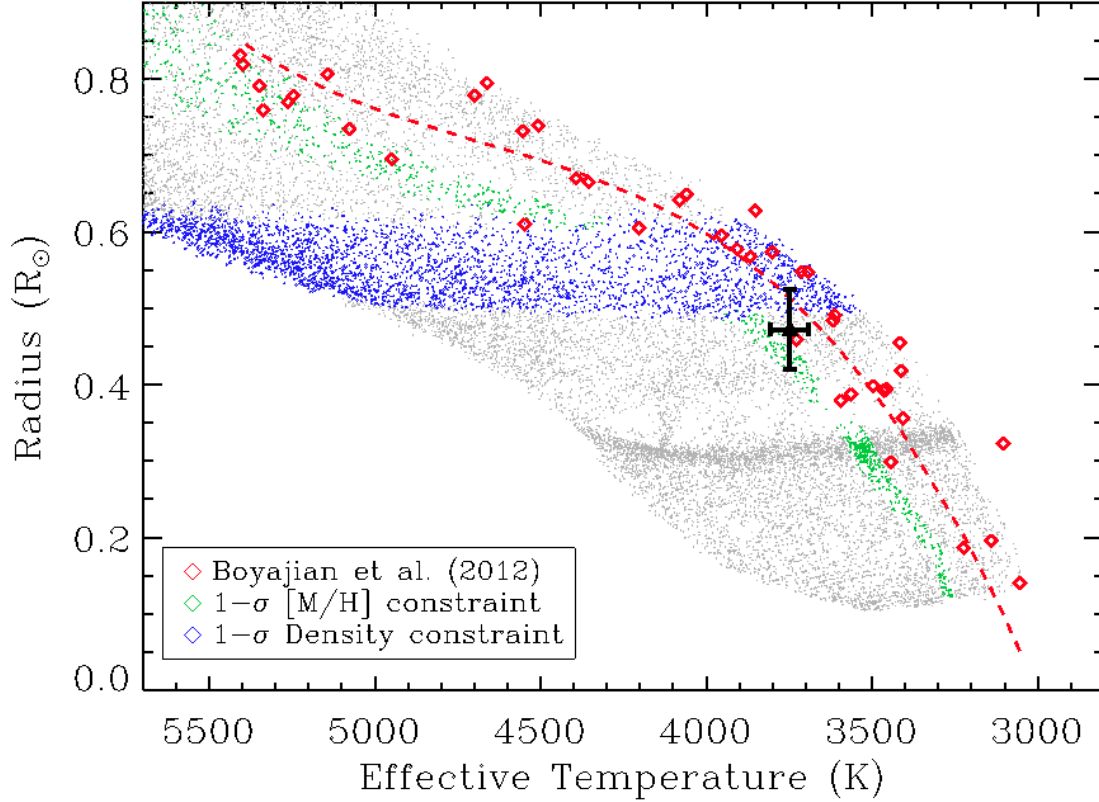


Figure S1. Stellar radius versus effective temperature for Dartmouth isochrones with metallicities ranging from -2.5 to +0.5 dex (grey). Green and blue points mark models within $1-\sigma$ of the spectroscopic metallicity and transit-derived mean stellar density, respectively. The black error bar indicates the derived position for Kepler-186. Red diamonds are interferometric measurements of single stars together with an empirical $R-T_{\text{eff}}$ relation (dashed line) (46).

3. Data preparation and transit modeling

We began our analysis of the Kepler observations using simple aperture photometry data (SAP_FLUX) contained in the light curve FITS files hosted at the MAST archive. These data contain both astrophysical variability and uncorrected instrumental systematic noise. We removed most instrumental signals by fitting ‘cotrending basis vectors’ (47, 48) (available from the MAST) to the Kepler time series data using the PyKE software (49). Given our goal was to characterize the planets, we removed astrophysical variability (mainly from the rotation of the star) and the remaining instrumental signal using a second order Savitzky-Golay filter with a window of 2 days. The planet transits were weighted zero in this filtering and we treated each observing Quarter of data independently (each Quarter typically includes about 3 months of data sampled at near-continuous 29.4 minute intervals). Finally we normalized the data and combined separate Quarters into a single time series, using Quarters Q0 - Q15 in our analysis.

Our transit model for Kepler-186 consists of five planets with transit profiles calculated using an analytic transit prescription (11) with a quadratic limb darkening law. The transit model parameters we sample are mean stellar density (ρ), photometric zeropoint, the two limb darkening parameters, a linear (γ_1) and quadratic term (γ_2), and for each planet: the midpoint of transit (T0), orbital period (P_{orb}), impact parameter (b) and eccentricity vectors $e \sin \omega$ and $e \cos \omega$, where e is eccentricity and ω is the argument of periastron. We also include an additional systematic uncertainty term (σ_s) as a model parameter that is added in quadrature with the quoted uncertainty in the Kepler data files (σ_e).

In the MCMC modeling the photometric zeropoint was assigned an unconstrained uniform prior as were the orbital period of the planets and the time of first transit. The prior on the impact parameter was uniform between zero and $(1+k)$ where k is the planet-to-star radius ratio and the prior on k was uniform between zero and 0.5. Parameterizing e and ω in terms of $e \sin \omega$ and $e \cos \omega$ enforces a linear prior on e (50). While the underlying eccentricity distribution of planets is poorly constrained, it is very unlikely that planets are preferentially in highly eccentric orbits. We assume a uniform prior in e which leads us to include a $1/e$ term as a prior to counteract the bias. The mean stellar density was assigned a Gaussian prior with mean and uncertainty constrained by the spectroscopic observations. For Kepler-186 the model stellar density is not strongly constraining allowing the data to dominate over the prior. Finally, the two limb darkening coefficients are assigned a Gaussian prior with expectation values computed by trilinearly interpolating over (T_{eff} , $\log(g)$ and Fe/H) tabular data derived with a least-squares method for the Kepler bandpass with Atlas model atmospheres (51). The width of the prior on the limb darkening coefficients was taken to be 0.1. We restricted the limb darkening to physical values (52). The Gaussian log-likelihood used function was

$$\log \mathcal{L} = -\frac{1}{2} \left\{ J \log 2\pi + \log \left[\sum_{j=1}^J (\sigma_{e,j}^2 + \sigma_s^2) \right] + \sum_{j=1}^J \frac{(x_j - \mu_j)^2}{\sigma_{e,j}^2 + \sigma_s^2} \right\}$$

where x_j is the j th data point in the flux time series with J total observations and μ is the model. We calculate a log-likelihood to help with numerical stability.

The affine invariant MCMC algorithm we apply involves taking N steps in an ensemble of M walkers and jump n is based on the $n-1$ position of the ensemble of walkers. We utilized 800 walkers taking 20,000 steps each for a total of 16 million samples.

Parameters derived from the marginalized posterior distributions of the parameters in our MCMC analysis are shown in Table S2. We found a mean stellar density of $4.92^{+0.89}_{-1.06}$ g cm⁻³ and limb darkening coefficients of $\gamma_1 = 0.295^{+0.077}_{-0.077}$ and $\gamma_2 = 0.461^{+0.097}_{-0.094}$.

We then derive from the Markov-chains and the probability distribution of the stellar parameters additional physical characteristics of the planets. The planetary radius is calculated from the posterior distribution of R_p/R_* multiplied by a normal distribution describing the stellar radius. The semi-major axis is derived using the formula

$$a = \left(\frac{P^2 G^* Q^*}{3\pi} \right)^{1/3} R_*$$

where P , Q and G (the gravitational constant) are in consistent units. The probability distribution of the semi-major axis, a , is computed element-wise in the above equation using the Markov-chain arrays. Finally, the insolation can be calculated independent of the stellar radius. The above equation can be manipulated to be in terms of a/R_* , then insolation (in Earth-Sun units) can simply be derived from

$$S = \left[(a/R_*)^{-2} T_*^4 \right] / \left[(a_{\oplus}/R_{\odot})^{-2} T_{\odot}^4 \right].$$

This derivation of insolation keeps all the correlations between parameters from the transit model intact and is not affected by uncertainties in the stellar luminosity and radius.

Table S2. Transit analysis (Median, +/- 1 σ uncertainty)

	b	c	d	e	f
Mid-transit Epoch T0 (BJD-2454833)	133.3304 +0.0013 -0.0013	174.3142 +0.0012 -0.0013	176.9045 +0.0014 -0.0015	153.8006 +0.0024 -0.0024	176.8183 +0.0064 -0.0068
Orbital Period P (days)	3.8867907 +0.0000062 -0.0000063	7.267302 +0.000012 -0.000011	13.342996 +0.000025 -0.000024	22.407704 +0.000074 -0.000072	129.9459 +0.0012 -0.0012
Impact parameter b	0.30 +0.20 -0.20	0.28 +0.20 -0.19	0.36 +0.19 -0.24	0.31 +0.20 -0.20	0.43 +0.19 -0.27
R_p/R_\star	0.02075 +0.00055 -0.00045	0.02424 +0.00056 -0.00047	0.02715 +0.00079 -0.00056	0.02465 +0.00065 -0.00055	0.02144 +0.00103 -0.00092
$e \cos \omega$	-0.00 +0.23 -0.24	-0.00 +0.23 -0.24	-0.00 +0.23 -0.25	0.00 +0.24 -0.24	-0.00 +0.30 -0.34
$e \sin \omega$	-0.04 +0.07 -0.17	-0.03 +0.07 -0.14	-0.03 +0.07 -0.17	-0.03 +0.07 -0.16	-0.01 +0.11 -0.21
$R_p (R_\oplus)$	1.07 +/-0.12	1.25 +/- 0.14	1.40 +/-0.16	1.27 +0.15 -0.14	1.11 +0.14 -0.13
Semimajor axis a (AU)	0.0343 +/- 0.0046	0.0520 +/- 0.0070	0.0781 +/- 0.010	0.110 +/-0.015	0.356 +/- 0.048
Insolation $S (S_\oplus)$	34.4 +6.3 -4.2	14.9 +2.7 -1.8	6.6 +1.2 -0.8	3.33 +0.61 -0.41	0.320 +0.059 -0.039

Note: The values reported are the median and the central 68% of the probability density. The median values are not intended to be self consistent but represent our knowledge of a parameter's distribution.

4. Kepler data validation

The first three planet candidates in this system, Kepler-186b-d, were detected in the first 4 months of Kepler data that include Quarters Q0 - Q2 (53). A 4th candidate, Kepler-186e, was detected in the Q1-Q6 data (54), and all four of these inner planets were confirmed using Q1 - Q8 data (9, 10). Kepler-186f was detected in the Q1-Q12 data set, but we used Q1 - Q15 data for our modeling.

Each planet candidate was individually examined to exclude obvious background eclipsing binary induced false positives (55). This included looking for differences in the depth of odd and even numbered transits, looking for shifts in the photo-center of the star during the transit and searching for secondary eclipses. All of the candidate planets orbiting Kepler-186 passed the vetting tests.

5. Follow-up observations

We undertook an extensive campaign to collect high-contrast images of Kepler-186 in order to establish whether a low mass binary companion to the primary was detectable or if there was a chance alignment of a field star with Kepler-186.

Kepler-186 was observed using the Differential Speckle Survey Instrument (DSSI) on the WIYN 3.5-m telescope on 20110911 in 692-nm and 880-nm filters (approximately *R* and *I*-band). No companions were detected between 0.2-2.0 arcsec. The $5\text{-}\sigma$ detection limit at 0.1 arcsec was 3.6 mag fainter than the target (throughout we will refer to the detection limit at the Δmag).

Kepler-186f was again observed with the DSSI instrument on 20130725, this time using the 8-m Gemini North telescope in the same filters as on the WIYN 3.5-m. Conditions were not optimal on the night when these observations were taken with high cirrus clouds limiting the contrast ratio at 0.2 arcsec to $\Delta\text{mag}=4.9$ at $5\text{-}\sigma$. No sources were detected within 0.03-2.0 arcsec of the target star.

On 20130624 Kepler-186 was observed using the natural guide star adaptive optics system with the NIRC2 camera on the Keck-II telescope. A series of *Ks*-band images were obtained using a three-point dither pattern. No nearby sources were detected between 0.2-5.0 arcsec of the target with a Δmag of 6.9 at 0.5 arcsec.

In Figure S2 we show the regions of parameter space that can be excluded based on speckle observations (left panel) and AO from Keck-II (right panel). Figure S3 shows all the parameter space that can be excluded for each planet candidate with high-contrast imaging constraints converted to the Kepler bandpass (56). The regions of ΔK_p -separation space where a false positive star cannot exist based on Kepler and follow-up imaging data are shaded green (speckle), pink (AO), blue (transit model) and yellow (Kepler centroid). The remaining parameter space, shown in white, cannot be excluded and must be accounted for in our false positive calculations.

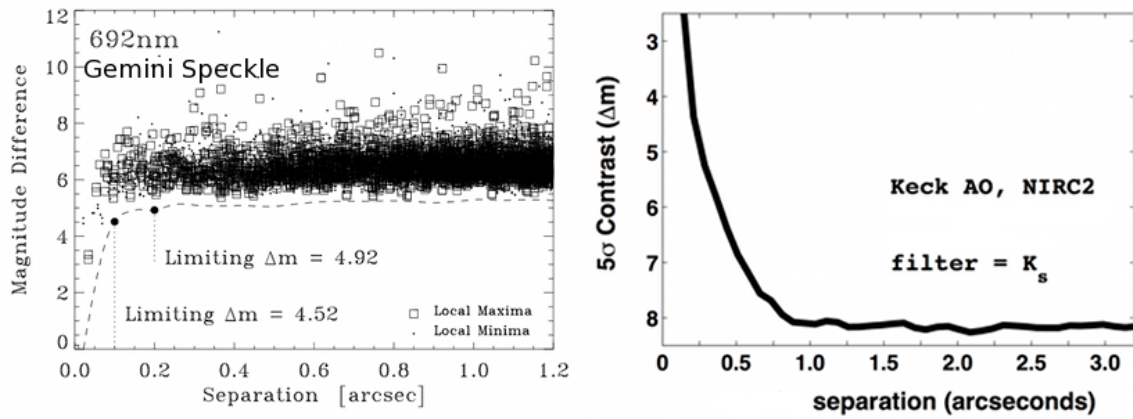


Figure S2. Ground-based follow-up observations. Speckle imaging data taken from the WIYN telescope is shown in the left panel and adaptive optics data from Keck II is shown on the right. Each panel shows the limiting magnitude difference as a function of separation where a false positive can be ruled out.

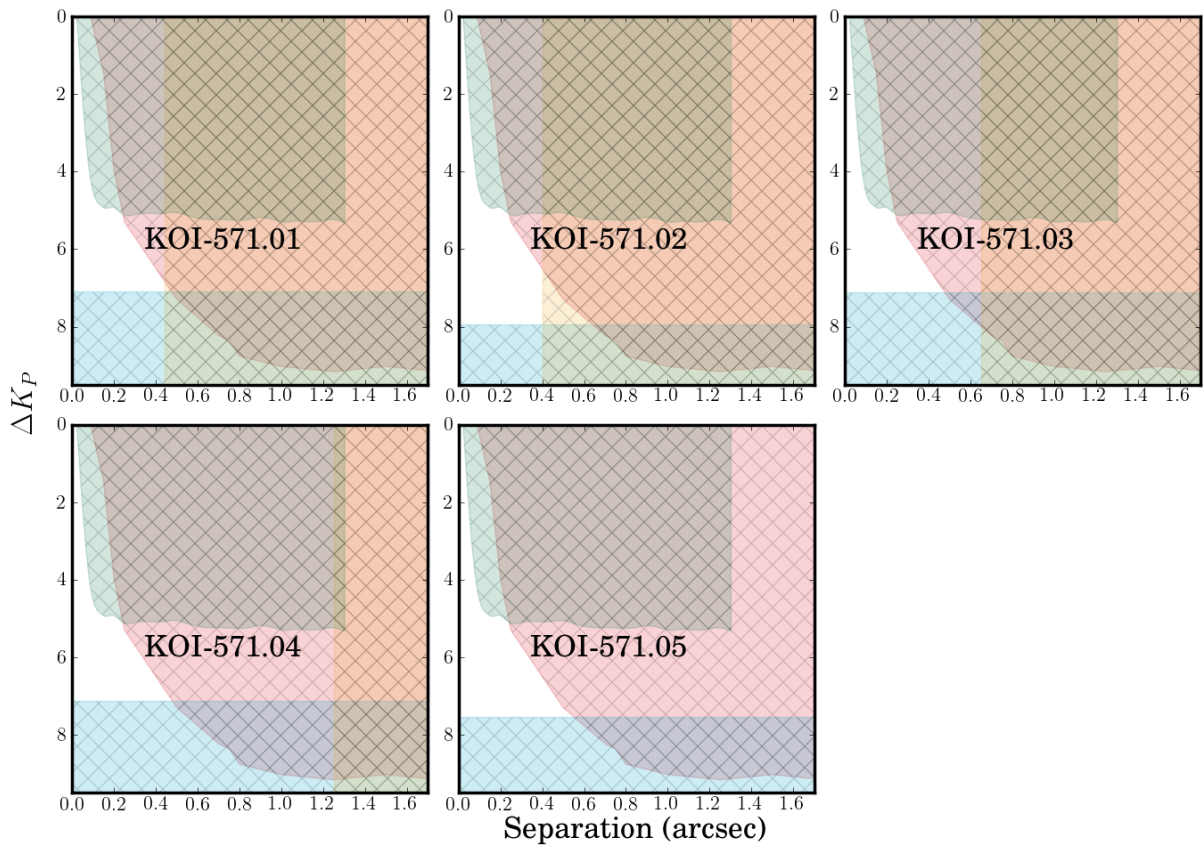


Figure S3. Exclusion zones for each of the planet candidates in the Kepler-186 system. Observational constraints rule out false positive inducing stars in all parts of the parameter space save for the white region. High-contrast imaging constraints have been transformed to apply to the Kepler bandpass.

We did not seek radial velocity observations, because a detection of a planet around a star this faint is beyond the capabilities of the current generation of radial velocity instruments.

6. False positive analysis

Given the available Kepler and follow-up observations, our goal was to determine the probability that the transit signals we detected were not transits of a planet across the face of Kepler-186. In this analysis we only consider Kepler-186f because the inner four planets have recently been validated as bona fide planets (9, 10).

Significant sources of false positives are background or foreground eclipsing binaries, planets orbiting a background or foreground star and planets orbiting a stellar binary companion to the target star. We first consider the case of a background eclipsing binary and background planetary systems. In this statistical analysis we will initially assume that Kepler-186f is the only candidate in the system and then apply a boost to the probability to account for the fact that false positives are significantly less common in multi-planet candidate systems.

We simulate the stellar population in a 1 square degree around Kepler-186 using the TRILEGAL galaxy model (57). From this we estimate the stellar density to be 8.8 million stars per square degree brighter than $K_p=32$ in a cone around Kepler-186. As shown in figure S3, we are able to exclude much of the available parameter space that background stars may reside in. We integrated the white region shown in the KOI-571.05 panel of Figure S3 with respect to the Galaxy model to arrive at an estimate of 0.01 stars hidden behind or in front of Kepler-186 that could in principle have a stellar or planetary companion that causes the transit-like signal we observe. We multiply this by the occurrence rate of non-contact eclipsing binaries or planets as seen in Kepler data (2.6%) to arrive at a final probability that the Kepler-186f transit is caused by an eclipsing binary of 2.6×10^{-4} . There were 145,000 dwarf stars observed with Kepler for transits but we can only find transit-signals the depth of Kepler-186f in 89% of these stars. Therefore, we estimate the rate of eclipsing binary or background planetary systems in systems such as this will occur 33 times in the Kepler data set. The false positive probability found via computing the ratio of the false positive probability to the a priori probability that Kepler-186f is a planet, found via looking at the number of Earth-sized planets found in Kepler data. To keep our calculations of the multiplicity boost valid, our planet prior probability is the number of Earth-sized planets in single planet systems found in the Q1-12 search of the Kepler data. There were 299 Earth-size planet candidates ($0.8 < R_{\oplus} < 1.25$) found in Q1-Q12 data, however, we expect 12.3% of these to be false positives (58) leaving 262 Earth-sized planets. Therefore, if Kepler-186f were a single planet system the probability that it were a false positive would be $[33/(262+33)] = 11.1\%$. These odds drop dramatically if we consider the multiplicity of the system. Accounting for multiplicity, the relative probability of a false positive drops by a factor of about 30 (59), yielding a confidence in the

planetary interpretation of 99.5%.

The second false positive scenario we consider is that of a planet orbiting a stellar companion to the primary star. Typically this scenario is the dominant source of false positives for small planets (58, 59). However, with multi-planet candidate hosting M-star primaries such as Kepler-186, we gain a strong constraint on the star that the planets' orbit from transit modeling. Here we assume that all planets orbit the same star but that star's properties are unknown. We repeated the transit modeling described in S3 but removed the mean stellar density and limb darkening priors (save for preventing them from exploring into unphysical parameters (52)) and diluted the transit depth appropriately to account for the light of the primary star. This allowed us to place an upper limit on the density of the star hosting the transits of 11.2 g/cc. Interpolating this onto Dartmouth isochrone models, we find a lower limit on the mass of the planet hosting star of $0.39 M_{\odot}$. Such a star would only be 0.5 mag fainter than the primary star.

A companion star to Kepler-186 would have to be within a projected distance of 4.2 AU of the primary otherwise our Gemini-North speckle observations would have detected the star. However, if the outer planet was orbiting the secondary it would only be dynamically stable if the closest approach of the stars was not less than 1.4 AU (22). We created a population of possible binary companions to the primary using a Monte Carlo simulation method. The distributions of binary separation, mass ratio and eccentricity were taken from the field star statistics (60). We adopted a binarity rate of 10% which is appropriate for exoplanet hosting binaries separated by less than 10 AU (21). From the sample of potential companions we removed all companions that would not be allowed based on observations or would cause the outermost planet to become unstable from dynamical interactions from the brighter star. We ran our simulations 10^7 times and an undetected companion was found on 445 occasions, an occurrence rate of 4.4×10^{-5} . The planet may still orbit the primary star, however, in the 445 cases with a feasible companion. We assigned a likelihood that the planet orbits the companion star that is proportional to the ratio of the probability to transit for the secondary relative to the primary star (a planet is less likely to transit a smaller star). This yields an occurrence rate of this false positive scenario of 2.1×10^{-5} per star observed by Kepler. An estimate of the occurrence rate in Kepler data of the scenario whereby the planet orbits a companion star can be estimated by multiplying the false positive probability per star by the number of stars hosting planet candidates, i.e. $(2.1 \times 10^{-5} \times 3601) = 0.075$ false positives. Compared to our a priori estimate of 417 for the occurrence rate of stars hosting at least one Earth-sized planet (there are 475 stars with at least one Earth-sized planet and we assume a false positive rate of 12.3%) our confidence that Kepler-186f orbits the primary star rather than an unseen companion is 99.98%.

7. Coplanarity

The relative durations of planets in a multi-planet candidate system can also provide information on whether all the planets orbit the same star. For a given planet with a central transit (impact parameter $b = 0$) and circular orbit, the transit duration (D) is proportional to $P^{1/3}$ (where P is the orbital period in days). If the scaled durations ($D/P^{1/3}$) of each planet in a system are equal, then it is highly likely that these planets orbit the same star (61). The scaled durations for the five planets of Kepler-186, all of which are consistent with having circular orbits, are shown in Figure S4 in order of ascending orbital period. The scaled durations are very similar among the planets, providing support that the signatures in the Kepler-186 light curve are due to five planets orbiting the same star. Interestingly, the scaled durations decrease slightly with planet orbital period, suggesting that they transit at increasing impact parameters. Increasing impact parameters as a function of orbital distance is expected if the planets lie in the same orbital plane, indicating the Kepler-186 planets are relatively coplanar.

Note that in order for the inner planet (b) to transit, we must view the system within a known angle of about 3.7 degrees, and in order for the outer planet (f) to transit, the viewing angle has the smaller range of only about 0.35 degrees. As a result, the planetary orbits are constrained to be nearly coplanar (within a few degrees). In comparison, circumstellar disks typically have scale heights (in the inner regions) of order $h/r \sim 0.05$, which implies co-planarity to about 3 degrees.

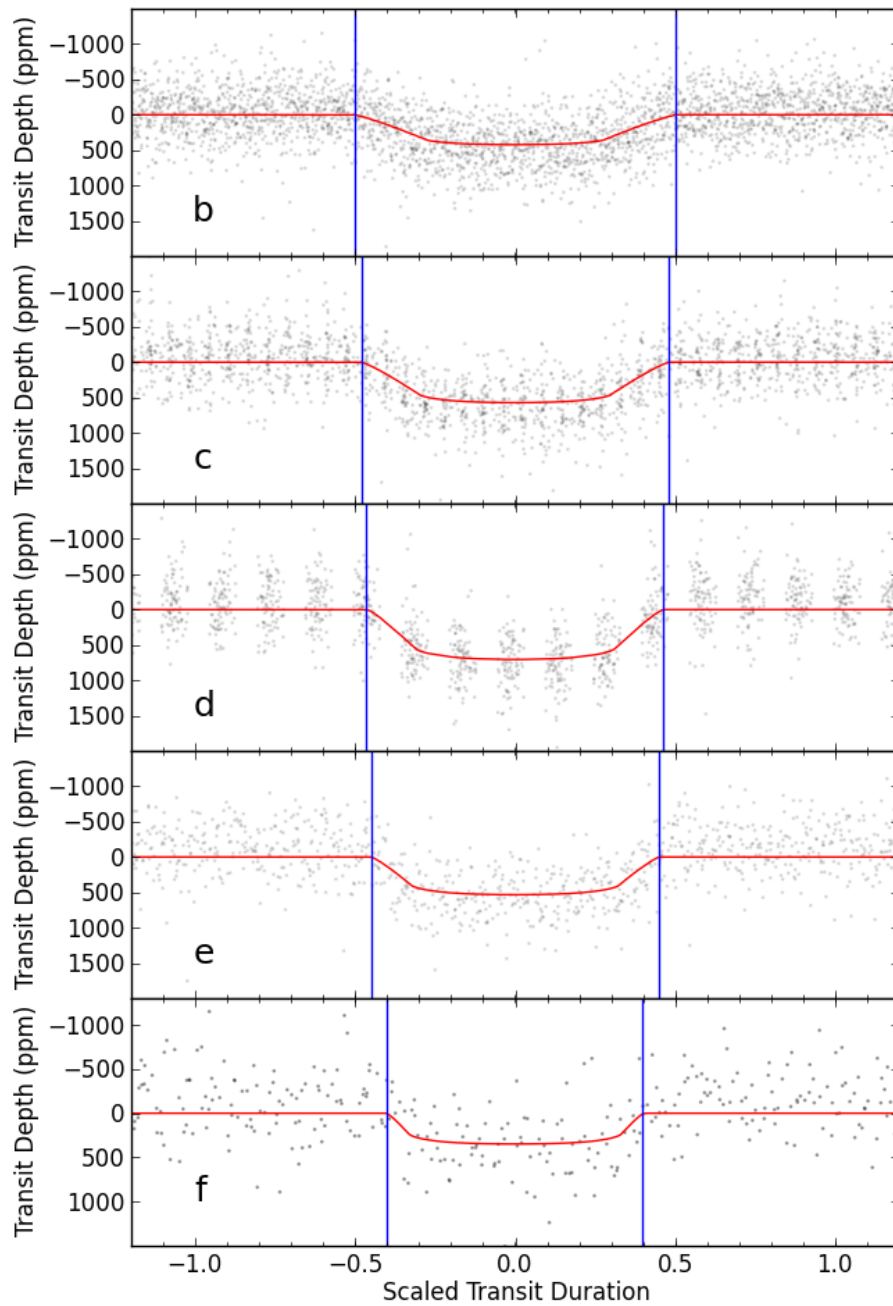


Figure S4. Normalized durations of the Kepler-186 planets. Each panel shows the folded light curve of a planet normalized by the cube root of the orbital period ($P^{1/3}$). This allows a direct comparison of the relative durations. If all of the durations are consistent, as they are in this system, it is highly likely that all planets orbit the same star.

8. Orbital Stability

A system of two planets in orbit around a star is dynamically stable if the objects are spaced by roughly 3.5 or more mutual Hill radii $R_{H,m}$ (62, 63). The mutual Hill radius is defined as $R_{H,m} = 1/2 (a_1 + a_2)[(m_1 + m_2)/3M_*]^{1/3}$, where subscripts 1 and 2 refer to the two planets, a is the orbital semimajor axis, m is the planet mass, and M_* is the stellar mass. A system of many planets must be more widely separated than a critical limit of 5-10 mutual Hill radii to ensure long-term stability (64, 65).

Although we don't have mass estimates for the Kepler-186 planets which are needed for our dynamical stability simulations, we assume they are terrestrial in nature using the following reasoning. All five planets around Kepler-186 have sizes less than $1.4 R_{\oplus}$, which thermal evolution models predict are too small to be dominated with a low density H/He gas envelope (23). Furthermore, any H/He envelope that may have been accreted was likely lost via photoevaporation early in the star's lifetime. With a measured rotation period of 34 days (66, 67) and no significant flaring observed in the Kepler light curve, Kepler-186 is likely older than about 4 Gyrs (68, 69) which is old enough such that the main phase of atmospheric erosion should have already occurred. If we assume a simple model of energy limited escape (3), and scale the UV flux to that of the UV-quiet Sun at the distance of Kepler-186f, then the estimated mass loss rate is about $10^{-4} M_{\oplus}/\text{Gyr}$. As a result, in a few Gyr, only a relatively small fraction of the planet's mass would be evaporated, but this change in mass corresponds to roughly 100 times the current mass of the atmosphere of Earth. These planets are much more likely to be composed of some combination of denser material (silicate rock, iron, and/or water). Table S3 lists the planets' masses for a wide range of plausible compositions using widely-used theoretical mass-radius relations (70).

Table S3. Range of plausible planet masses (in M_{\oplus})

	Pure Ice (H ₂ O)	Pure Rock (Silicate)	Earth-like	Pure Iron
Planet b	0.28	0.90	1.26	3.23
Planet c	0.46	1.56	2.24	6.30
Planet d	0.66	2.38	3.50	10.00
Planet e	0.48	1.66	2.38	6.76
Planet f	0.32	1.02	1.44	3.77

The dynamical inter-planet spacing depends on the planets' true masses. Planets b and c are

dynamically closest together and planets e and f are the most widely spaced. Lower-density, lower-mass planets are more widely spaced in dynamical terms (mutual Hill radii). For pure ice, planets b and c are separated by $12 R_{H,m}$, but this value decreases with increasing planet mass to $7 R_{H,m}$ for Earth-like compositions and just $5 R_{H,m}$ for pure iron planets. The gap between planets e and f is wide enough to fit another planet. For ice-rock-Earth-iron planets, the gap is 45-30-26-19 mutual Hill radii wide.

To examine the dynamical stability of the Kepler-186 system, we ran a suite of N-body simulations of the five-planet system for the full range of planetary compositions. Given the weak constraints on the planets' eccentricities and longitudes of pericenter, we sampled a range of orbital phases and included initial eccentricities up to 0.05. In all cases the systems were stable for the 0.1 Myr duration. We ran 10 longer-term simulations (without tides or general relativity) with pure iron planets, all of which were stable for 100 Myr, the duration of the simulations.

We stress that close-packed multi-planet systems display chaotic dynamics, so that the question of stability must be addressed statistically. As a result, a great deal of additional dynamical work can be done to explore the long term stability of this system. Such work would result in stronger constraints (upper limits) on the (as yet unknown) planetary masses.

9. Formation

The planets in our solar system are thought to have formed in situ by accreting local material from a protoplanetary disk of gas and dust that surrounded the newly formed Sun (71). The discovery of hundreds of short-period exoplanets and the diversity of their sizes, masses and system architecture has shed new light on classical planet formation theories. Many systems require some form of inward migration of mass during their formation (28, 29), or planet-planet scattering after they formed to bring them inwards, to explain their observed properties.

We performed a suite of N-body numerical simulations of late-stage accretion around a star like Kepler-186 in order to shed light on the types of protoplanetary disks that would be needed to form planetary systems like Kepler-186b-f in situ. We examine populations of 20 planetary embryos and/or 200-400 planetesimals spread between 0.02-0.5 AU. The surface density profile was varied between r^{-1} and $r^{-2.8}$, and the total mass in solids ranged from 6-10 M_{\oplus} . Our simulations begin at the epoch of planet formation just after the gas in the disk is dissipated, and each system was integrated with the *Mercury* hybrid integrator (72), which treats collisions as perfect mergers, for 10 Myr using a 0.2 day timestep.

Figure S5 shows the outcome of eight of the N-body simulations. Simulations that began with

more massive initial disks ($10 M_{\oplus}$) and steeper surface density profiles ($r^{2.5}$) were most successful in reproducing the broad mass-orbital radius distribution of the Kepler-186 system. Disks with this much mass so close to their star or with such steep surface density profiles, however, are not commonly observed (30), suggesting that the Kepler-186 planets likely formed from material that underwent some inward migration in the earlier stages of formation while gas was still present in the disk, or perhaps were perturbed inwards by a distant planet or star.

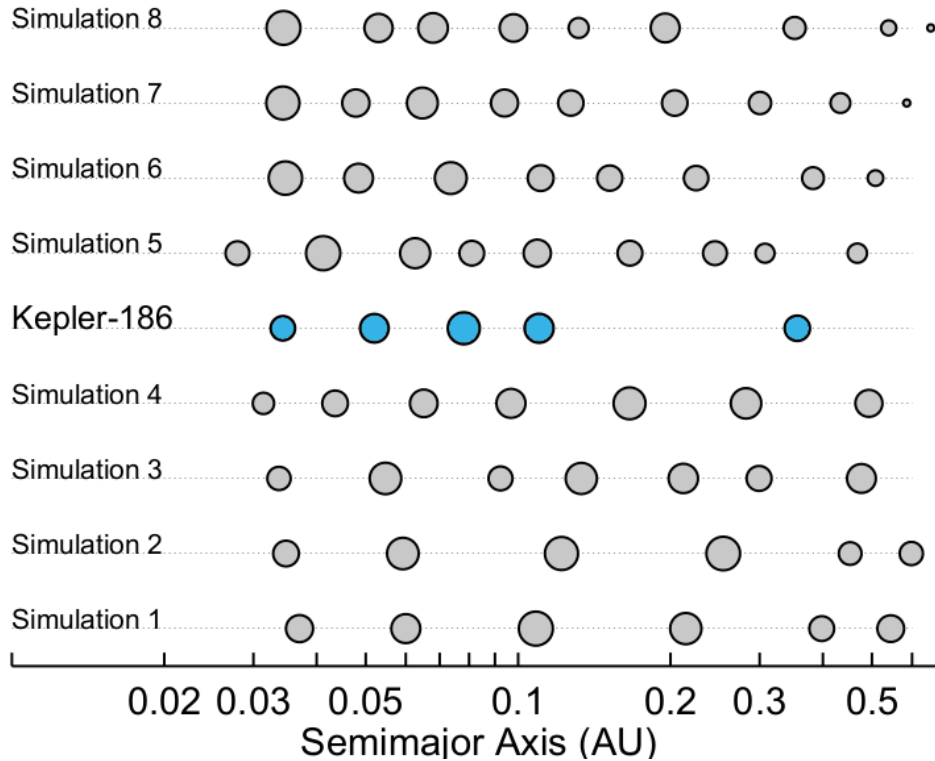


Figure S5. Final planetary systems that formed in eight of our simulations. Each symbol represents a final planet and the symbol size is proportional to its radius derived from theoretical mass-radius relations (73). The Kepler-186 planets are shown in blue. Simulations 1-4 began with a surface density profile of $r^{-1.8}$ and simulations 5-8 began with a steeper profile of $r^{-2.7}$. All simulations formed 1-2 planets in orbits between those of Kepler-186e and Kepler-186f.

Regardless of how these planets formed, these simulations demonstrate that a sixth planet could in theory remain stable in-between the orbits of known planets e and f (0.15-0.35 AU). Could such a planet exist in the system but not transit? For that to be the case, that planet would need to have a modest inclination of at least a few degrees with respect to the common plane of the other planets. A collision or scattering event after the dissipation of the gaseous disk could produce such an inclination. It would then be a simple coincidence that planet f's orbit is aligned with the inner ones whereas this extra planet's is not. Or, if this extra planet is relatively lower-mass than the other

planets then its secular oscillations in inclination can simply reach a higher amplitude than the other planets, decreasing the probability of observing it in common transit with the other planets.